Catalysis
Science & Technology

Cite this: *Catal. Sci. Technol.*, 2012, **2**, 1367–1374

www.rsc.org/catalysis

PAPER

Fabrication of magnetic mesoporous manganese ferrite nanocomposites as efficient catalyst for degradation of dye pollutants

Banalata Sahoo,[a] Sumanta Kumar Sahu,[b] Suryakanta Nayak,[c] Dibakar Dhara[a] and Panchanan Pramanik*[a]

Received 16th January 2012, Accepted 11th March 2012
DOI: 10.1039/c2cy20026k

In this study, mesoporous silica encapsulated with magnetic $MnFe_2O_4$ nanoparticles is synthesized by a solvothermal method. The synthetic route is feasible and widely applicable. The obtained products have been characterized by an X-ray powder diffraction (XRD) pattern, field emission scanning electron microscopy (FESEM), transmission electron microscopy (TEM), high-resolution TEM (HRTEM) and nitrogen adsorption–desorption isotherm measurements. The synthesized magnetic mesoporous $MnFe_2O_4$ nanoparticles are monodispersed with a mean diameter of 200 nm, and have an obvious mesoporous silica shell of ~20 nm. The surface area of magnetic mesoporous $MnFe_2O_4$ nanocomposites is 423 m^2 g^{-1}. The nanoparticles are superparamagnetic in nature at room temperature and can be separated by an external magnetic field. This magnetic mesoporous material is used as a catalyst for the degradation of methyl orange dye. The merits of the effect under different conditions like pH, temperature, light and sonolysis have been evaluated by investigating the degradation of azo dye. The mesoporous $MnFe_2O_4$ nanocomposites have effective adsorption of dyes inside the porous network followed by degradation with the central magnetite core and regeneration of the catalyst with the help of a simple magnet for successive uses.

Introduction

Mesoporous materials, having large surface area and uniform pore distribution, have been extensively studied for their widespread purpose in the fields of adsorption, catalysis, sensors, semiconductor and separation.[1–4] Over the past few years, a large amount of work has been done on the magnetic nanoparticles due to their magnetism properties and they are applied extensively in different fields.[5–9] If one could combine the advantages of mesoporous and magnetic nanoparticles to construct a nanocomposite with high surface area and magnetic separability, then the nanocomposites can be used for a wide range of applications. Now these mesoporous magnetic materials have been widely investigated for many potential applications such as electronic, magnetic, catalytic and biological sensing properties over the last few years.[10–13]

Recently, it was also reported that mesoporous magnetic materials are used in the degradation of aromatic organic compounds in industrial wastewater.[14] Among various magnetic nanoparticles, Fe_3O_4 nanoparticles are mostly used for preparing magnetic mesoporous materials.

In recent days decolourisation of synthetic dyes as potential pollutants has attracted considerable attention in environmental science. From the economical point of view, the removal of these dyes is of significant importance. There are many methods established for decolourisation of the synthetic dyes. One of the suitable methods to deal with the problem seems to be the use of catalytic oxidation with hydrogen peroxide. The catalysts decompose H_2O_2 yielding highly reactive hydroxyl radicals, and are able to decolourise the synthetic dyes. Recently, several systems for homogeneous and heterogeneous catalytic decomposition of hydrogen peroxide and production of hydroxyl radicals have been developed.[15–18] Numerous studies have been carried out to find efficient heterogeneous systems, including zeolites, clays and oxide materials.[19] The most used heterogeneous catalysts are based on magnetic mixed iron oxide nanoparticles.

Recently, mesoporous magnetic nanocomposites have received much attention since these composites not only retain the catalytic activity of the metal nanoparticles but also possess the photocatalytic activity.[20–22] In this regard, several investigators have employed standard nanoparticle preparation methods for dye degradation. Recently, Fe_3O_4@C@Cu_2O magnetic core–shell composites with bean-like morphology have been explored to have visible-light-photocatalytic activity for the degradation of organic pollutants.[23] Panda *et al.* demonstrated catalytic activity of the Fenton-like mesoporous Fe_2O_3–SiO_2 composite towards successful decolourisation of methyl orange.[24] In addition,

[a] *Nanomaterials Laboratory, Department of Chemistry, Indian Institute of Technology Kharagpur, W.B., 721302, India. E-mail: blsahoo.chem@gmail.com, pramanik1946@gmail.com; Fax: +91 3222-255303; Tel: +91 9775664551*
[b] *Department of Applied Chemistry, Indian School of Mines, Dhanbad 826004, India*
[c] *Rubber Technology Centre, Indian Institute of Technology, Kharagpur, India*

Zhang *et al.* have synthesized superparamagnetic Fe_3O_4 nanoparticles as catalysts for the catalytic oxidation of phenolic and aniline compounds from aqueous solution.[25] Fe_3O_4–poly(3,4-ethylene-dioxythiophene) core–shell nanoparticles as heterogeneous Fenton catalysts have been synthesized by acid etching-mediated chemical oxidation polymerization. These core–shell nanoparticles have demonstrated outstanding catalytic performance for the degradation of Reactive Black 5 and Orange II.[26] However, to the best of our knowledge, the magnetic nanosized $MnFe_2O_4$ mesoporous composite has not been reported yet. The main objective of the present work is to investigate the catalytic effect of heterogeneous magnetically separable nanocomposites on decolourisation of synthetic dyes by hydrogen peroxide. Although detection of intermediates is very important during the degradation of dye, we are more interested in how much dye has degraded in the presence of nanocomposites and H_2O_2 under different conditions like temperature, pH, heat and in the presence of sunlight. We believe that in a real industrial application, total dye degradation is more important than the detection of intermediates. In this paper, we have reported the synthesis of magnetic $MnFe_2O_4$ mesoporous particles by a solvothermal process and their characterization by diverse techniques. A typical azo dye, namely methyl orange (MO), has been used as a model dye to investigate degradation properties by adsorption experiments. Meanwhile, it is easy to separate the catalyst for recycling uses after the reaction is finished. The catalytic effect of the synthesized $MnFe_2O_4$ mesoporous composites has been studied under different conditions like effect of pH, temperature, light and sonolysis.

2. Experimental

2.1. Materials

Anhydrous ferric chloride ($FeCl_3$), manganese chloride ($MnCl_2{\cdot}4H_2O$), tetraethyl orthosilicate (TEOS), methyl orange (MO), cetyltrimethylammonium bromide (CTAB), ammonia and ethanol were purchased from Merck. Hydrogen peroxide (30%, w/v), sodium acetate, ethylene glycol, ammonium nitrate were also procured from Merck, Germany. All the chemicals were of reagent grade and were used without further purification. Water used throughout the experiment is milli Q ultrapure water.

2.2. Synthesis of manganese ferrite ($MnFe_2O_4$) nanoparticles

Superparamagnetic $MnFe_2O_4$ nanoparticles were prepared by a solvothermal method in an autoclave. For the synthesis of $MnFe_2O_4$ nanoparticles, a mixture of $MnCl_2$ (0.416 g, 2.1 mmol), $FeCl_3$ (0.683 g, 4.2 mmol), and sodium acetate (0.5 g) was dissolved in 40 ml ethylene glycol and stirred vigorously for 1 h at room temperature to obtain a homogenous solution. After vigorous stirring of the mixture for 1 h, the homogeneous solution was transferred to a Teflon-lined stainless steel autoclave (90 ml capacity), sealed, and heated to 160 °C for 24 h. After cooling the autoclave to room temperature, the $MnFe_2O_4$ nanoparticles were repeatedly washed with ethanol and distilled water, and then dried under vacuum at 60 °C for 12 h.

2.3. Silica coating over magnetite nanoparticles

For thin silica coating on the surface of $MnFe_2O_4$ nanoparticles, 0.1 g of $MnFe_2O_4$ nanoparticles were first ultrasonically treated with 50 ml of 0.1 M HCl aqueous solution for 10 min. The magnetic particles were then separated and washed with deionized water. Then the particles were homogeneously dispersed in a mixture of 80 ml ethanol, 20 ml deionized water and 1 ml concentrated ammonia aqueous solution (28%) for 30 min. Then 0.03 g tetraethyl orthosilicate (TEOS) was added dropwise to the above-mentioned mixture. After magnetically stirring at room temperature for 6 h, the product was separated and washed with ethanol and deionized water.

2.4. Synthesis of $MnFe_2O_4$ mesoporous composites

$MnFe_2O_4$ mesoporous composites were prepared according to the literature with little modification.[27] The silica coated ferrite particles were redispersed in a mixed solution containing 0.3 g cetyltrimethylammonium bromide (CTAB), 80 ml deionized water, 70 ml absolute ethanol and 1.2 ml concentrated ammonia aqueous solution (28%) for 30 min to get a homogenous dispersion. The solution mixture was stirred continuously followed by the addition of 0.4 g TEOS and the reaction was continued for 6 h. After 6 h stirring at room temperature, the product was collected by magnetic decantation and repeatedly washed with ethanol and deionized water. The structure-directing agent CTAB was thereafter removed with the exchange of surfactant molecules with alcoholic solution of ammonium nitrate. The whole synthesis procedure is presented in Scheme 1. The nanoparticles were dispersed in ethanolic solution containing 0.3 g NH_4NO_3 and the mixture was stirred at 60 °C. The products were recovered by magnetic separation, washed with ethanol followed by drying at 60 °C, and used as catalyst for dye degradation.

2.5. Dye degradation study

For dye degradation study, a stock solution of 0.6 mg ml^{-1} MO was prepared in milli Q water. For each decolourisation study, 1 ml of stock solution was treated with 2 ml of H_2O_2 (30%, w/v) and 20 mg of catalyst. The total volume of the mixture was adjusted to 10 ml with milli Q water. The decrease in absorbance of the supernatant solution was checked by spectrophotometric measurements at 463 nm using a Shimadzu UV-1700 spectrophotometer. The degree of decolourisation (DD)

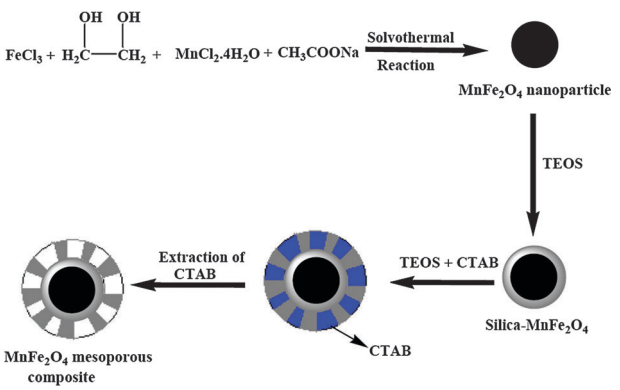

Scheme 1 Schematic illustration of the fabrication of magnetic $MnFe_2O_4$ mesoporous nanocomposites.

of the sample was determined by using the relation DD% = $(C_i - C_t)/C_i \times 100$ where C_i is the initial absorbance of the sample and C_t is the absorbance at time t. The methyl orange degradation study was performed by varying conditions like pH and temperature. The photochemical and sonochemical effects on dye degradation were also studied under similar experimental conditions.

2.6. Characterizations

The phase formation and crystallographic state of uncoated as well as functionalized magnetic nanoparticles were determined by using a Phillips PW 1710 X-ray diffractometer (XRD) with Ni-filtered Cu-K_α radiation (λ = 1.54 Å). The presence of surface functional groups was investigated by Fourier Transform Infrared (FTIR) spectroscopy. The samples were prepared in KBr medium in the range of 400–4000 cm^{-1} with a model Thermo Nicolet Nexus FTIR (model 870). The size and morphology of the nanoparticles were observed by high-resolution transmission electron microscopy (HRTEM) (JEOL 3010, Japan) and Phillips CM 200 was used for performing the field emission scanning electron microscopy (FESEM). The nanoparticles were thoroughly dispersed in water by ultra-sonication and a drop of the solution was placed on a carbon coated copper grid. Magnetic measurements were performed using a SQUID-VSM instrument (Evercool SQUID VSM DC Magnetometer). The dye degradation study was monitored by UV-Vis spectroscopy on a Shimadzu UV-1700 spectrophotometer. The surface area, pore size and pore distribution were determined by using a N_2 adsorption–desorption instrument (Quantachrome Corporation, Quantachrome Autosorb Automated Gas Sorption System).

3. Results and discussion

3.1. Synthesis of $MnFe_2O_4$ mesoporous nanocomposites

Monodispersed manganese ferrite nanoparticles are synthesized by using $MnCl_2$ and $FeCl_3$ as precursors, NaOAc as base and ethylene glycol is selected as the solvent. Here ethylene glycol behaves both as reducing and surface capping agent for the controlled synthesis of monodispersed manganese ferrite nanoparticles. The synthesis procedure for the ferrite nanoparticle involves the formation of $Fe(OH)_3$ and $Mn(OH)_2$ from their salt precursors which are finally transferred to the growth of $MnFe_2O_4$ nanoparticles.[28] The schematic preparation process of $MnFe_2O_4$ mesoporous composites is shown in Scheme 1.

The pristine manganese ferrite nanoparticles are spherical in shape having a mean diameter of 80–90 nm. The silica coated magnetic $MnFe_2O_4$ mesoporous nanocomposites are prepared through a soft template assisted route. CTAB is used as soft template and structure-directing agent, which is later removed for the uniform generation of pores in the material. The removal of surfactant CTAB is carried out by exchanging the surfactant with ammonium nitrate solution. The thin layer of inner silica coating on ferrite nanoparticles protects the metal core from harsh reaction conditions and offers stability to the inner magnetite core. The porous silica structure helps in the recognition of guest molecules and allows easy access of guest molecules inside the porous network.[29] Our synthetic material shows good mesoporous behaviour with ordered porous structure.

3.2. X-Ray diffraction

The successful synthesis of $MnFe_2O_4$ nanocomposites and their crystallinity are evident from the XRD pattern presented in Fig. 1.

The peaks are observed at 2θ = 30.195°, 35.543°, 43.217°, 53.60°, 57.067°, 62.665° and 71.15° which represent the Bragg reflections from the (220), (311), (400), (422), (511), (440) and (533) planes respectively. The diffraction peaks in Fig. 1 determine the cubic nature of nanoparticles and all the peaks match well with the standard XRD pattern of $MnFe_2O_4$ nanoparticles (JCPDS card No. 10-0319). The broadening of XRD peaks delineates the crystalline nature of particles. From the XRD pattern of the $MnFe_2O_4$ mesoporous composites (shown in Fig. 1b and c), the main peaks are observed to be similar to those of the pure $MnFe_2O_4$ particles (Fig. 1a), which reveals that the crystal structure of $MnFe_2O_4$ is well retained after the silica coating process. The presence of silica on the $MnFe_2O_4$ mesoporous composites is observed from the low angle XRD pattern (inset). A broad peak is observed at an angle between 2° and 3° which confirms the presence of silica on the mesoporous material.

3.3. FTIR study

FTIR spectroscopy is further used to characterize the silica-coated magnetic nanoparticles shown in Fig. 2. Pure manganese ferrite nanoparticles show a characteristic peak at 3427 cm^{-1}, revealing the presence of residual hydroxyl groups, and the peak at 584 cm^{-1} is attributed to Fe–O bond vibration. The high density of hydrophilic –OH groups facilitates the magnetic manganese ferrite nanoparticles with excellent aqueous dispersibility and stability, which can further provide magnetic nanoparticles to functionalize with silica precursors. Magnetic mesoporous manganese ferrite shows a characteristic peak at 1088 cm^{-1} which corresponds to Si–O bond stretching of Si–O–Si. From the Si–O characteristic peak the successful coating of silane on magnetic nanoparticles has been confirmed. But very small peaks at 2862 cm^{-1} and 2935 cm^{-1} are observed in each case, which confirms that these peaks are due

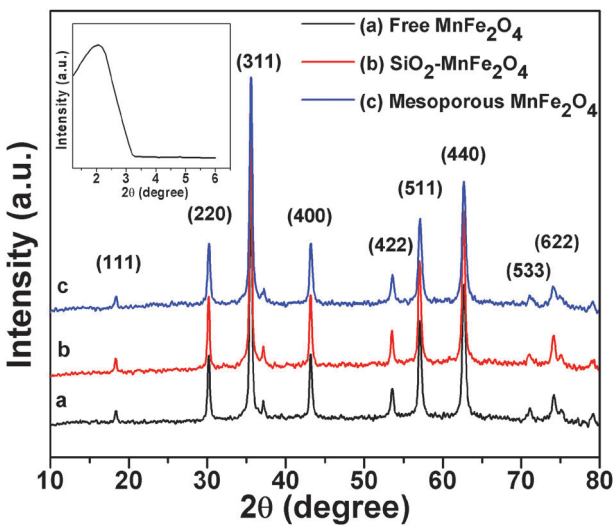

Fig. 1 The wide-angle XRD patterns of the (a) as-prepared $MnFe_2O_4$ nanoparticles, (b) silica–$MnFe_2O_4$ nanoparticles, (c) $MnFe_2O_4$ mesoporous composites and the low-angle XRD curve (inset) of $MnFe_2O_4$ mesoporous composites.

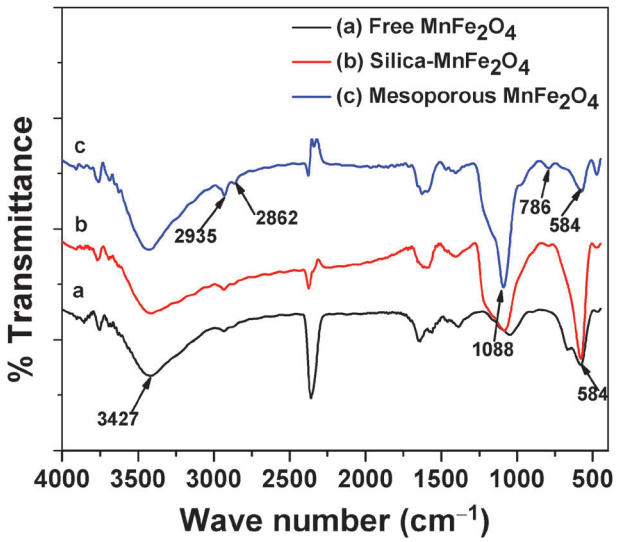

Fig. 2 FT-IR spectra of the (a) $MnFe_2O_4$ nanoparticles, (b) Silica–$MnFe_2O_4$ nanoparticles and (c) $MnFe_2O_4$ mesoporous composites.

to the trace amount of physically adsorbed ethylene glycol (–CH_2– stretching) on the ferrite surface during magnetic nanoparticle synthesis.

3.4. Surface area measurements

The porous framework of the material is also established from the N_2 adsorption–desorption isotherm curve and the surface area is measured by the BET surface area analyzer. Fig. 3 corresponds to the nitrogen adsorption–desorption isotherms and HK pore size distribution curves of $MnFe_2O_4$ mesoporous nanocomposites. The removal of soft template CTAB results in the porous structure of the material. The $MnFe_2O_4$ mesoporous composites show short-range mesoscopic ordering character. N_2 adsorption–desorption isotherms exhibit a type-IV curve for the mesoporous material. The surface area of $MnFe_2O_4$ mesoporous composites is much higher compared to other reports.[30,31] The mesopore size distribution exhibits a sharp peak centered at the mean value of 1.7–1.9 nm, indicating a uniform mesopore. The BET surface area and pore volume are calculated to be 423 $m^2\ g^{-1}$ and 0.15 $cm^3\ g^{-1}$, respectively. The small pore size of the mesoporous material endows higher surface area.

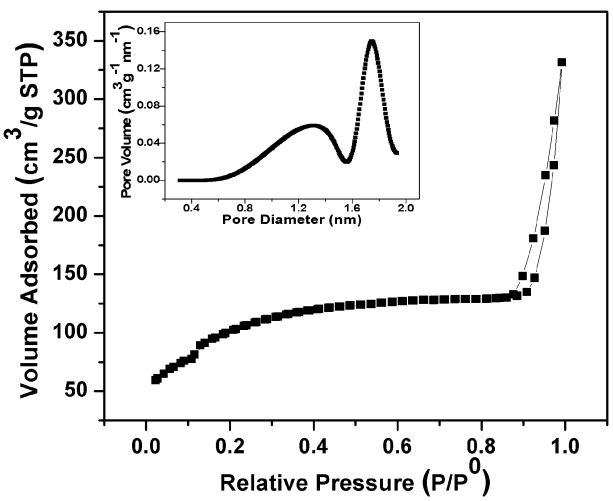

Fig. 3 N_2 adsorption–desorption isotherms and the mesopore size distribution curve (inset) of $MnFe_2O_4$ mesoporous composites.

3.5. Size and morphology study

The morphology, shape and size of nanoparticles are obtained by FESEM and TEM analysis. Both FESEM and TEM images (Fig. 4) illustrate the spherical morphology of $MnFe_2O_4$ mesoporous composites.

The FESEM image illustrates the well-defined spherical morphology of individual particles (Fig. 4a). The particles are uniform in size, having smooth surface, and diameters of particles from FESEM image are obtained to be about 200 nm. The composition of the $MnFe_2O_4$ mesoporous composites is obtained from EDS analysis, which is presented in Fig. 4b. The EDS spectrum of $MnFe_2O_4$ mesoporous composites confirms the presence of Fe, Mn, Si and O elements, validating the purity of the material. The TEM image of pristine $MnFe_2O_4$ nanoparticles which are spherical in shape having a mean diameter of 90–100 nm is shown in Fig. 4c. The selected area electron diffraction pattern clearly reveals the polycrystalline nature of nanoparticles, which is shown Fig. 4d. The crystallinity of the nanoparticle is well observed from the selected area electron diffraction pattern. Apart from BET measurements the porous nature of the material is clearly

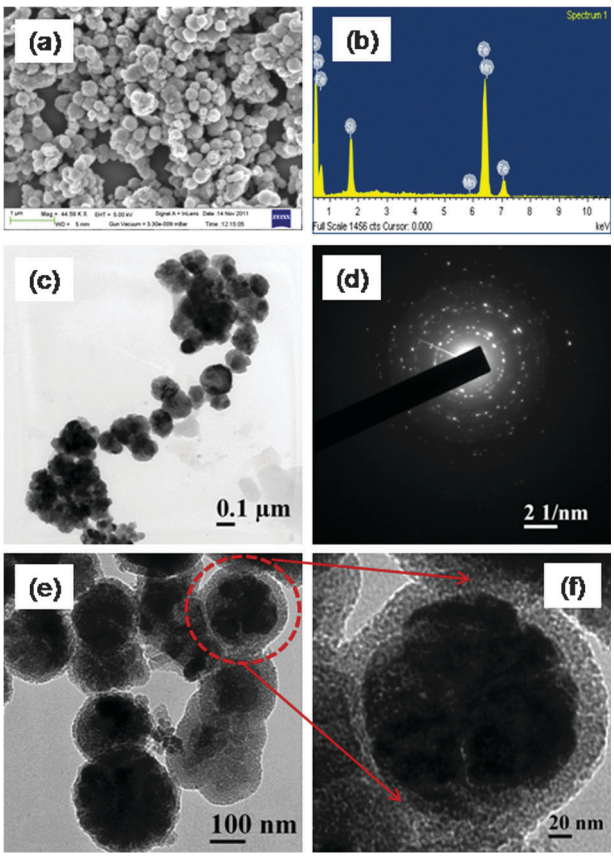

Fig. 4 (a) FESEM image and (b) EDX spectrum of the $MnFe_2O_4$ mesoporous composites, (c) TEM of $MnFe_2O_4$ nanoparticles (d) SAED of the $MnFe_2O_4$ mesoporous composites, (e) HRTEM of $MnFe_2O_4$ mesoporous composites (f) a single particle at a high resolution.

observed from TEM analysis. Fig. 4e represents the TEM of $MnFe_2O_4$ mesoporous nanocomposites. From the TEM picture the mesoporous structure is clearly observed and particles are monodisperse in nature. A single porous particle at a higher magnification value is presented in Fig. 4f. The thickness of the outer silica shell is found to be around 20 nm. Each particle contains a black magnetic core with the outer mesoporous silica shell.

3.6. VSM study

The magnetic property of $MnFe_2O_4$ nanoparticles is obtained by field dependent magnetization measurements as shown in Fig. 5. Fig. 5a and b depict the magnetization *versus* applied magnetic field plots for the magnetic $MnFe_2O_4$ nanoparticles and $MnFe_2O_4$ mesoporous composites at 300 K. The absence of hysteresis loop indicates the superparamagnetic nature of the $MnFe_2O_4$ nanoparticles and the composites. The saturated magnetization value for pure $MnFe_2O_4$ is found to be 103 emu g^{-1}, whereas for $MnFe_2O_4$ mesoporous composites it is 69 emu g^{-1}. The magnetization value obtained for pure $MnFe_2O_4$ nanoparticles is much higher compared to other methods reported previously. The reduced saturation magnetization of the $MnFe_2O_4$ mesoporous composites is due to the silica coating which lowers the magnetization value due to magnetic dipolar interaction.

3.7. Catalytic performance on methyl orange

The degradation of MO was studied by both the as-synthesized $MnFe_2O_4$ nanoparticles and $MnFe_2O_4$ mesoporous composites under identical reaction conditions in the presence of H_2O_2 at room temperature. The comparison of the MO degradation performance is presented in Fig. 6a. It is observed that the degradation efficiency of $MnFe_2O_4$ mesoporous composites is 10% higher as compared to native $MnFe_2O_4$ nanoparticles. This is due to higher surface area and more pore distribution, which allows the dye molecules to come into contact with the active site of the particles. A typical degradation of methyl orange by mesoporous composites is presented in Fig. 6b. In the figure the UV-Vis spectrum of MO degradation by $MnFe_2O_4$ mesoporous composites is presented. Curve 1 represents initial MO solution

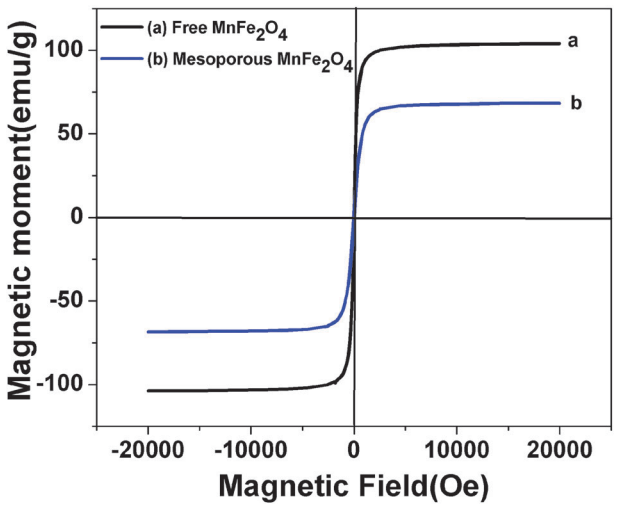

Fig. 5 Magnetization curve of both $MnFe_2O_4$ nanoparticles and $MnFe_2O_4$ mesoporous composites.

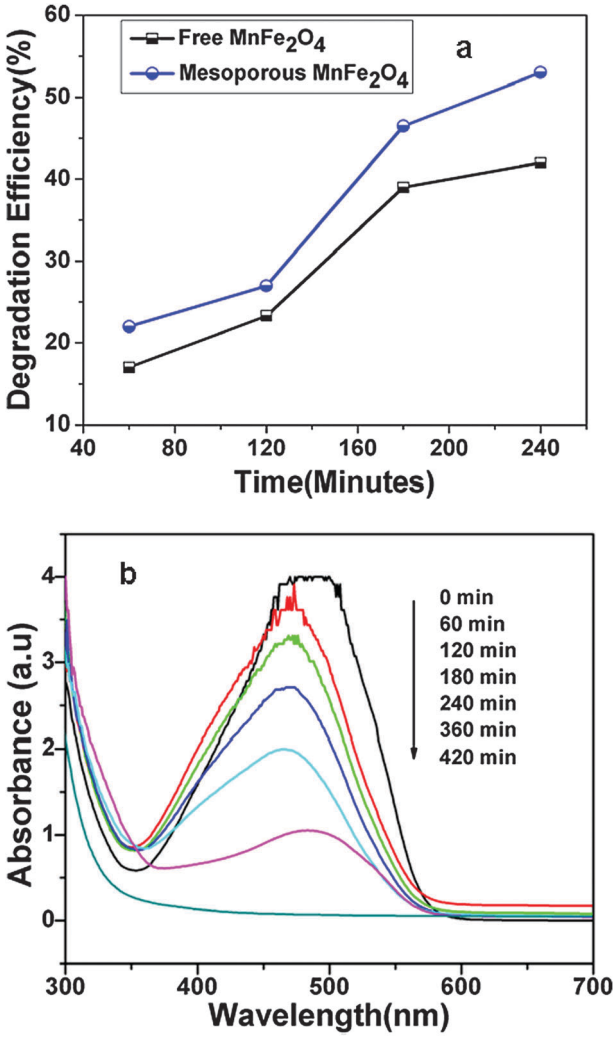

Fig. 6 (a) Comparison of degradation efficiency of MO by both $MnFe_2O_4$ nanoparticles and $MnFe_2O_4$ mesoporous composites (b) UV-Vis curve of MO degradation by $MnFe_2O_4$ mesoporous composites. MO degradation is carried out at 27 °C, 2 ml of 30% H_2O_2, 1 ml of 0.6 mg ml^{-1} MO solution, 20 mg catalyst, pH of the solution = 5.0.

(concentration 0.6 mg ml^{-1}) at 0 min. The degradation is carried out at room temperature. Upon increasing the reaction time, the degradation efficiency increases and the degradation curves are presented successively. After 420 min the MO solution is completely degraded by $MnFe_2O_4$ mesoporous composites. In order to investigate the role of the catalyst, the control experiment has been performed in the absence of the catalyst, only taking dye solution and H_2O_2. No decolourisation of dye solution has been observed for a time period of 3 h in the absence of the catalyst. The role of $MnFe_2O_4$ in dye degradation is due to the presence of Mn metal in the magnetite structure which strongly favours the peroxide decomposition.[32,33] Yonghong Ni *et al.* reported that the incorporation of Mn^{2+} into TiO_2 nanoparticles enhanced the photocatalytic activity of TiO_2 nanoparticles.[34] Costa *et al.* reported that the Mn^{2+} metal ion like Fe^{2+} ions played an active role in the decomposition of H_2O_2 to generate OH radical species.[32] T.D. Nguyen *et al.*[35] reported that Fe_2MnO_4/AC–H has a much higher MO degradation efficiency compared to Fe_3O_4/AC–H. The possible

reaction for dye degradation is due to the electron transfer processes within the $MnFe_2O_4$ particles. The proposed mechanism for H_2O_2 decomposition on $MnFe_2O_4$ is outlined below. $MnFe_2O_4$ nanoparticles have inverse spinel magnetite structure. So in inverse spinel magnetite Mn^{2+} occupies the octahedral site and Fe^{3+} ions occupy both octahedral and tetrahedral sites. Mn^{2+} ions on the surface of inverse spinel magnetite structure play an important role in the decomposition of H_2O_2 and generation of O_2 species. The possible mechanism for H_2O_2 decomposition by Mn^{2+} ions is outlined below.

$$Mn^{2+} + H_2O_2 \rightarrow Mn^{3+} + HO^{\bullet} + OH^{-} \quad \text{(i)}$$

$$H_2O_2 + HO^{\bullet} \rightarrow H_2O + HOO^{\bullet} \quad \text{(ii)}$$

$$Mn^{3+} + HOO^{\bullet} \rightarrow Mn^{2+} + H^{+} + O_2 \quad \text{(iii)}$$

$$Fe^{3+} + HOO^{\bullet} \rightarrow Fe^{2+} + O_2 + H^{+} \quad \text{(iv)}$$

The above generated O_2 molecule and $^{\bullet}OH$ react with organic dye (RH).

$$R\text{–}H + HOO^{\bullet} \rightarrow X + H_2O + CO_2 \quad \text{(v)}$$

X = degraded organic product.

The excess manganese tripositive ion generated in the reaction medium may scavenge the hydroxyl and oxy hydroxyl radicals generated in the reaction. The scavenging effect of hydroxyl and oxy hydroxyl radicals is inhibited as the Mn^{3+} generated in the system is reduced by the Fe^{2+} ion. According to Costa *et al.*[32] the reduction of Mn^{3+} by Fe^{2+} is thermodynamically favourable as shown by the following equations:

$$Fe^{3+} + 1e^{-} \rightarrow Fe^{2+},\ E^{\circ} = 0.77\ V \quad \text{(vi)}$$

$$Mn^{3+} + 1e^{-} \rightarrow Mn^{2+},\ E^{\circ} = 1.51\ V \quad \text{(vii)}$$

The higher reduction potential of Mn^{3+} ions compared to Fe^{3+} ions promotes the reduction of Mn^{3+} ions and produces Mn^{2+} ions which again continue the catalytic cycle of H_2O_2 decomposition.

$$Fe^{2+} + Mn^{3+} \rightarrow Fe^{3+} + Mn^{2+},\ E^{\circ} = 0.73\ V \quad \text{(viii)}$$

The above thermodynamically possible reaction provides a suitable path for dye degradations. Therefore, considering relatively higher degradation rate of the composite adsorbent than pristine $MnFe_2O_4$ nanoparticles, it can be used as a promising alternative adsorbent to decolourise the dye. The impact of various parameters on MO dye degradation efficiency is discussed below.

3.8. Effect of light

In order to investigate the photochemical influence on the degradation ability of $MnFe_2O_4$ mesoporous composites, the dye solution was kept in sunlight and the decolourisation was observed at 30 min time interval. The effect of sunlight on photo degradation ability of $MnFe_2O_4$ mesoporous composites is presented in Fig. 7. This shows the degradation efficiency of MO with irradiation time. It is observed that, in the absence of light, when performed in the dark, nearly very less degradation of MO was observed. Under sunlight irradiation for 180 min, nearly 98% of the MO molecules are degraded. In addition, Fenton reaction hydroxyl radicals are also generated upon

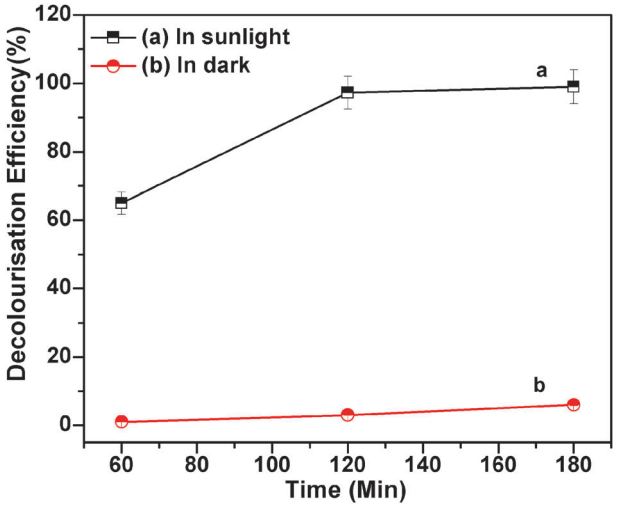

Fig. 7 MO degradation by $MnFe_2O_4$ mesoporous composites (a) in the presence of sunlight (keeping the solution under sunlight), 2 ml of 30% H_2O_2, 1 ml of 0.6 mg ml^{-1} MO solution, 20 mg catalyst, pH of the solution = 5.0; (b) in the dark (temperature = 25 °C), 2 ml of 30% H_2O_2, 1 ml of 0.6 mg ml^{-1} MO solution, 20 mg catalyst, pH of the solution = 5.0.

exposure of H_2O_2 to sunlight. The reaction describing the production of $HO^{\bullet}$ is presented below.

$$H_2O_2 + h\nu \rightarrow 2\ HO^{\bullet} \quad \text{(ix)}$$

$$H_2O_2 + HO^{\bullet} \rightarrow HO_2^{\bullet} + HO \quad \text{(x)}$$

$$H_2O_2 + HO_2^{\bullet} \rightarrow HO^{\bullet} + H_2O + O_2 \quad \text{(xi)}$$

So the combination of photon (sunlight) and mesoporous $MnFe_2O_4$ nanocomposites produces more number of hydroxyl radicals and enhances the degradation capability of MO dye over a short time range. Subsequently, to know the active role of the catalyst, the control experiment was carried out in the absence of catalyst under sunlight irradiation for the same time as above. In the absence of catalyst, nearly 20% of MO degradation is observed. This is due to the degradation of H_2O_2 under sunlight, which produces reactive radical species and degrades the MO dye. But the combined effect of catalyst and hydrogen peroxide is reflected for MO degradation under sunlight. Dye solution is quickly degraded in the presence of sunlight and catalyst. In addition to the role of sunlight in reactive radical species generation, the role of $MnFe_2O_4$ mesoporous composites in the same is well observed. The combined effect plays a significant role in MO degradation.

3.9. Effect of temperature

There have been many reports on the effect of temperature on degradation of dye with various kinds of nanocomposites. Recently Zhang *et al.* successfully synthesized Fe_3O_4 magnetic nanoparticles as a catalyst and investigated the effect of temperature to remove phenol and aniline from aqueous solution.[36] However, this approach seems to deserve an obvious result that the dye degradation increases with the increase in temperature. Here the degradation efficiency with temperature is determined by varying the temperature of the solution as shown in Fig. 8.

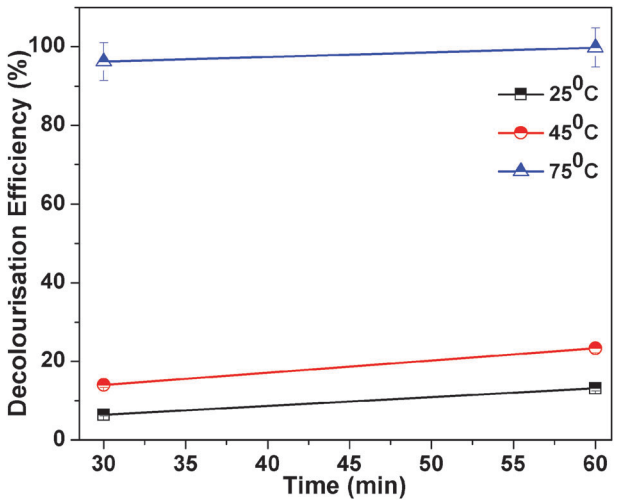

Fig. 8 MO degradation occurs at three different temperatures and other conditions remain the same. The three temperatures are 25 °C, 45 °C and 75 °C, 2ml of 30% H_2O_2, 1 ml of 0.6 mg ml^{-1} MO solution, 20 mg catalyst, pH of the solution = 5.0.

From the figure it is clearly observed that degradation efficiency increases with temperature. We have checked the degradation rate of MO at three different temperatures, that is, low (25 °C), moderate (45 °C) and high (75 °C). It was observed at lower temperatures that around 10% of MO is degraded after 60 min, with further rise in temperature at 45 °C, 20% MO is degraded. But at 75 °C, 99% degraded at the same time. The control experiment has been carried out for MO degradation in the absence of catalyst. In the absence of catalyst, a negligible amount of dye has degraded under the same reaction conditions. So temperature has an important role in the decolourisation of MO.

3.10. Effect of pH

The solution pH is one of the significant parameters affecting the degradation of dye onto the adsorbent. Here the dye degradation was carried out by $MnFe_2O_4$ mesoporous composites by varying the pH ranges from 2 to 12 as shown in Fig. 9. The pH of dye solution was adjusted with 0.1 M HCl and 0.1 M NaOH solution. It was observed that with particular pH solution more amount of dye has degraded. The degradation of methyl orange is higher at lower pH. The maximum decolourisation occurs at pH 2.0. At lower pH the surface of magnetic mesoporous manganese ferrite becomes positive which allows more number of MO molecules (negatively charged dye) on its surface and facilitates the degradation process. At higher pH (pH > 6.0) the degradation performance of MO decreases. The MO degradation is highest at pH 2.0. About 90% of MO is degraded at pH 2.0 after 350 min. However at higher pH (pH > 6.0) the degradation performance of MO decreases. The effect of pH on MO degradation was observed by other researchers.[37–39] All have reported that at lower pH more amount of dye degraded. Feng *et al.* also reported that the initial solution pH strongly affects the catalytic degradation of dye.[40] They have reported that the best photo-catalytic activity for the heterogenous Fenton reaction of orange II was observed at an initial solution pH of 3.0 and the activity of the catalysts decreases as the initial solution pH increases.

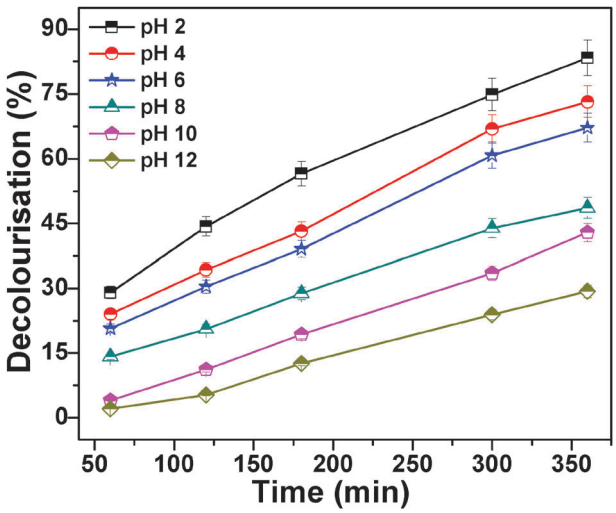

Fig. 9 MO degradation is carried out at different pHs and other conditions remain the same. The different pHs are 2.0, 4.0, 6.0, 8.0, 10.0, 12.0, 2 ml of 30% H_2O_2, 1 ml of 0.6 mg ml^{-1} MO solution, 20 mg catalyst and temperature is 28 °C.

3.11. Effect of sonication

The sonochemical technology is widely used for the destruction of organic pollutants. Here the degradation efficiency of the MO was investigated by the effect of sonication in the presence of bare $MnFe_2O_4$ nanoparticles and $MnFe_2O_4$ mesoporous composites. Compared with pure ferrite nanoparticles the porous ferrite nanoparticles show nearly 10% higher degradation efficiency. The degradation efficiency is again enhanced for porous ferrite nanoparticles upon sonication. The effect of sonication on MO degradation is illustrated in Fig. 10.

Degradation efficiency has been enhanced to nearly 26% upon sonication over a time period of 300 min. The sonolysis experiments were carried out with a 42 kHz (frequency) radiofrequency power 130 W sonolysis setup of Ultrasonic

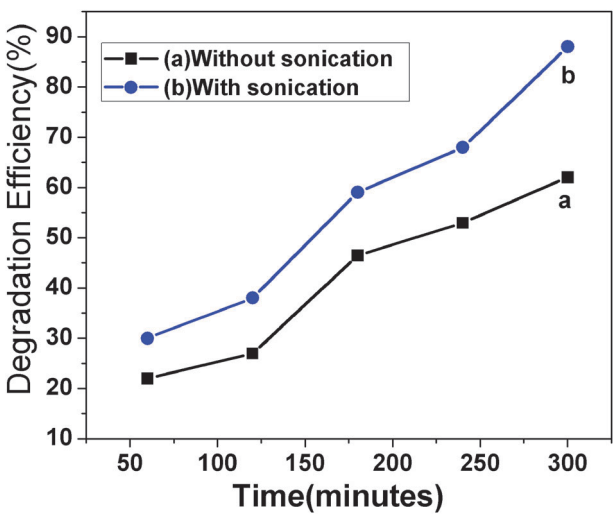

Fig. 10 MO degradation is carried out (a) without sonication, 2 ml of 30% H_2O_2, 1 ml of 0.6 mg ml^{-1} MO solution, 20 mg catalyst, pH of the solution = 5.0 (b) with sonication, 2 ml of 30% H_2O_2, 1 ml of 0.6 mg ml^{-1} MO solution, 20 mg catalyst, pH of the solution = 5.0.

Energy Systems (Bransonic, MTH-2510). Sonication generates radicals from H_2O_2. Under ultrasonic irradiation, the thermal decomposition of H_2O_2 in the cavitation bubble helps in the formation of reactive radicals. The combined effect of sonolysis and Fenton reaction generates more amount of hydroxyl radical species which in turn enhances the degradation efficiency of dye. Like sunlight, sonication has the ability to produce $^{\bullet}H$ and $^{\bullet}OH$ radicals from H_2O_2 (Naomi L. *et al.*).[41] 35% Degradation of naphthol blue black (an azo dye) was observed upon sonication (Naomi L. *et al.*) during the time period of 12 h. The $MnFe_2O_4$ mesoporous composites showed better degradation behaviour probably due to their high specific surface area and porosity.

3.12. Reusability of catalyst

The reusability of the catalyst was further investigated by separating the catalyst using an external magnet. The recovered nanocomposites were recycled five times for degradation of fresh methyl orange solution without significant loss of catalytic activity. At the end of each cycle the catalyst was washed with distilled water 3 times followed by drying in an oven. For subsequent repetitive cycles, the catalyst shows the same degradation performance as in the case of the initial one.

4. Conclusions

We have demonstrated an adsorption study of methyl orange on monodispersed magnetic mesoporous manganese ferrite nanocomposites (200–300 nm) synthesized by a solvothermal method. The synthesized nanocomposites matched well with the magnetite phase as obtained from powder XRD analysis and have a specific surface area of 423 $m^2\ g^{-1}$. This degradation phenomenon could be attributed to the porous structure of the catalyst which adsorbs the dye molecules followed by decolourisation by central magnetic $MnFe_2O_4$ nanoparticles. The MO degradation was high at low pH (pH 2.0) and decreased with the increase in pH. The process of decolourisation of MO is found to be optimum in an acidic pH. The degradation efficiency of MO is enhanced by sonication and photolysis under sunlight. MO degradation performance is better observed at higher temperature (75–80 °C) than normal temperature (25–30 °C). Finally, we have fruitfully designed a catalyst, which shows the properties of adsorption, degradation, easy catalyst isolation and reusability in one system.

Acknowledgements

The authors gratefully acknowledge Council of Scientific and Industrial Research (CSIR) New Delhi for financial support and IIT Kharagpur for research facilities.

References

1 W. Zhao, J. Gu, L. Zhang, H. Chen and J. Shi, *J. Am. Chem. Soc.*, 2005, **127**, 8916–8917.
2 D. P. Wang and H. C. Zeng, *Chem. Mater.*, 2011, **23**, 4886–4899.
3 Y. Deng, D. Qi, C. Deng, X. Zhang and D. Zhao, *J. Am. Chem. Soc.*, 2008, **130**, 28–29.
4 X. Kang, Z. Cheng, C. Li, D. Yang, M. Shang, P. Ma, G. Li, N. Liu and J. Lin, *J. Phys. Chem. C*, 2011, **115**, 15801–15811.
5 G. Chouhan, D. Wang and H. Alper, *Chem. Commun.*, 2007, 4809–4811.
6 M. Takafuji, S. Ide, H. Ihara and Z. Xu, *Chem. Mater.*, 2004, **16**, 1977–1983.
7 T. Sen, I. J. Bruceb and T. Mercerc, *Chem. Commun.*, 2010, **46**, 6807–6809.
8 D. K. Yi, S. T. Selvan, S. S. Lee, G. C. Papaefthymiou, D. Kundaliya and J. Y. Ying, *J. Am. Chem. Soc.*, 2005, **127**, 4990–4991.
9 S. Gai, P. Yang, P. Ma, D. Wang, C. Li, X. Li, N. Niua and J. Lin, *J. Mater. Chem.*, 2011, **21**, 16420–16426.
10 Q. Cheng, V. Pavlinek, A. Lengalova, C. Li, T. Belza and P. Saha, *Microporous Mesoporous Mater.*, 2006, **94**, 193–199.
11 S. Tao, C. Wang, W. Ma, S. Wu and C. Meng, *Microporous Mesoporous Mater.*, 2012, **147**, 295–301.
12 Q. Meng, W. Su, X. Hang, X. Li, C. He and C. Duan, *Talanta*, 2011, **86**, 408–414.
13 A. Bordoloi, N. T. Mathew, F. Lefebvre and S. B. Halligudi, *Microporous Mesoporous Mater.*, 2008, **115**, 345–355.
14 B. C. Kim, J. Lee, W. Um, J. Kim, J. Joo, J. H. Lee, J. H. Kwak, J. H. Kim, C. Lee, H. Lee, R. S. Addleman, T. Hyeon, M. B. Gui and J. Kim, *J. Hazard. Mater.*, 2011, **192**, 1140–1147.
15 O. A. Makhotkina, S. V. Preis and E. V. Parkhomchuk, *Appl. Catal., B*, 2008, **84**, 821–826.
16 W. Luo, L. Zhu, N. Wang, H. Tang, M. Cao and Y. She, *Environ. Sci. Technol.*, 2010, **44**, 1786–1791.
17 A. Rodrıguez, G. Ovejero, J. L. Sotelo, M. Mestanza and J. Garci, *Ind. Eng. Chem. Res.*, 2010, **49**, 498–505.
18 S. Papi, D. Vujevi, N. Koprivanac and D. Sinko, *J. Hazard. Mater.*, 2009, **164**, 1137–1145.
19 F. Duarte, F. J. Maldonado-Hodar, A. F. Perez-Cadenas and L. M. Madeira, *Appl. Catal., B*, 2009, **85**, 139–147.
20 L. Kao, T. Hsu and K. Cheng, *J. Colloid Interface Sci.*, 2010, **341**, 359–365.
21 Y. Noda, B. Lee, K. Domen and J. N. Kondo, *Chem. Mater.*, 2008, **20**, 5361–5367.
22 J. C. Yu, L. Zhang, Z. Zheng and J. Zhao, *Chem. Mater.*, 2003, **15**, 2280–2286.
23 S. K. Li, F. Z. Huang, Y. Wang, Y. H. Shen, L. G. Qiu, A. J. Xie and S. J. Xu, *J. Mater. Chem.*, 2011, **21**, 7459–7466.
24 N. Panda, H. Sahoo and S. Mohapatra, *J. Hazard. Mater.*, 2011, **185**, 359–365.
25 S. Zhang, X. Zhao, H. Niu, Y. Shi, Y. Cai and G. Jiang, *J. Hazard. Mater.*, 2009, **167**, 560–566.
26 S. Shin, H. Yoon and J. Jang, *Catal. Commun.*, 2008, **101**, 78–182.
27 C. Wang, S. Tao, W. Wei, C. Meng, F. Liu and M. Han, *J. Mater. Chem.*, 2010, **20**, 4635–4641.
28 S. Xuan, F. Wang, Y. X. J. Wang, J. C. Yua and K. C. F. Leung, *J. Mater. Chem.*, 2010, **20**, 5086–5094.
29 S. Tao, C. Wang, W. Ma, S. Wu and C. Meng, *Microporous Mesoporous Mater.*, 2012, **147**, 295–301.
30 P. Yang, Z. Quan, Z. Hou, C. Li, X. Kang, Z. Cheng and J. Lin, *Biomaterials*, 2009, **30**, 4786–4795.
31 H. Tian, J. Li, Q. Shen, H. Wang, Z. Hao, L. Zou and Q. Hu, *J. Hazard. Mater.*, 2009, **171**, 459–464.
32 R. C. C. Costa, M. F. F. Lelis, L. C. A. Oliveira, J. D. Fabris, J. D. Ardisson, R. R. V. A. Rios, C. N. Silva and R. M. Lago, *J. Hazard. Mater. B*, 2006, **129**, 171–178.
33 P. Baldrian, V. Merhautova, J. Gabriel, F. Nerud, P. Stopka, M. Hruby and M. J. Benes, *Appl. Catal., B*, 2006, **66**, 258–264.
34 Y. Ni, Y. Zhu and X. Ma, *Dalton Trans.*, 2011, **40**, 3689–3694.
35 T. D. Nguyen, N. H. Phan, M. H. Do and K. T. Ngo, *J. Hazard. Mater.*, 2011, **185**, 653–661.
36 S. Zhang, X. Zhao, H. Niu, Y. Shi, Y. Cai and G. Jiang, *J. Hazard. Mater.*, 2009, **167**, 560–566.
37 S. Chatterjee, S. Chatterjee, B. P. Chatterjee, A. R. Das and A. K. Guha, *J. Colloid Interface Sci.*, 2005, **288**, 30–35.
38 A. Mittal, A. Malviya, D. Kaur, J. Mittal and L. Kurup, *J. Hazard. Mater.*, 2007, **148**, 229–240.
39 H. Y Zhu, R. Jiang, L. Xiao and W. Li, *J. Hazard. Mater.*, 2010, **179**, 251–257.
40 J. Feng, X. Hu and P. Lock Yue, *Water Res.*, 2006, **40**, 641–646.
41 N. Stock, J. Peller, K. Vinod Gopal and P. V. Kamat, *Environ. Sci. Technol.*, 2000, **34**, 1747–1750.

